

Texture Mapping 3D Models of Indoor Environments with Noisy Camera Poses

Anonymous 3DIMPVT submission

Paper ID ****

Abstract

Automated 3D modeling of building interiors is useful in applications such as virtual reality and environment mapping. Applying textures to these models is an important step in generating photorealistic visualizations of data gathered by modeling systems. The localization of cameras in such systems often suffer from inaccuracies, resulting in visible discontinuities when different images are projected adjacently onto a plane for texturing. We propose two approaches for reducing discontinuities during texture mapping, one to robustly accomodate images of all orientations, and one to take advantage of optimal situations where images have uniform orientation. The effectiveness of our approaches will be demonstrated on two indoor datasets.

1. Introduction

Three-dimensional modeling of indoor environments has a variety of applications such as training and simulation for disaster management, virtual heritage conservation, and mapping of hazardous sites. Manual construction of these digital models can be time consuming, and as such, automated 3D site modeling has garnered much interest in recent years.

The aim of this paper is to present a solution for texture mapping the 3D models generated by indoor modeling systems, with specific attention given to a human-operated system with high camera pose errors and great variance in camera locations.

The first step in automated 3D modeling is the physical scanning of the environment's geometry. An indoor modeling system must be able to recover camera poses within an environment while simultaneously reconstructing the 3D structure of the environment itself. This is known as the simultaneous localization and mapping (SLAM) problem, and is generally solved by taking readings from laser range scanners, cameras, and inertial measurement units (IMUs) at multiple locations within the environment.

Mounting such devices on a human-carried platform provides unique advantages over vehicular-based systems in

terms of agility and portability. Unfortunately, human-operated systems also result in much larger localization error. As a result, common methods for texture mapping generally produce poor results, as later shown in Sections 2 and 3. Before discussing how to overcome these challenges, we first provide an overview of the backpack modeling system from which our test data has been obtained.

Our backpack-mounted modeling system contains five 2D laser range scanners, two cameras, and an orientation sensor. The laser scanners are mounted orthogonally and have a 30-meter range and a 270° field of view. The two cameras are equipped with fisheye lenses, reaching an approximately 180° field of view, and are mounted with one facing left and the other facing right. These cameras take images at the rate of 5 Hz. The orientation sensor provides orientation parameters at a rate of 180 Hz.

With the laser scanners active, the human operator wearing the backpack takes great care to walk a path such that every wall in the desired indoor environment is traversed and scanned lengthwise at least once.

Using data gathered by the onboard sensors and multiple localization and loop-closure algorithms, the backpack is first localized over its data collection period, and a 3D point cloud of the surrounding environment is constructed based on the laser scanner readings relative to the backpack [2, 6, 7]. Approximate normal vectors for each point in the point cloud are then calculated by gathering neighboring points within a small radius and processing them through principal component analysis. These normal vectors allow for the classification and grouping of adjacent points into structures such as walls, ceilings, floors, and staircases. A RANSAC algorithm is then employed to fit polygonal planes to these structured groupings of points, resulting in a fully planar model [9]. This model, consisting of multiple 2D polygonal planes in 3D space, along with the set of images captured by the backpack's camera, can be considered the input to our texture mapping problem.

The remainder of the paper is organized as follows. Section 2 describes the general problem of texture mapping and examines two simple mapping approaches and their shortcomings. Section 3 demonstrates two previous attempts

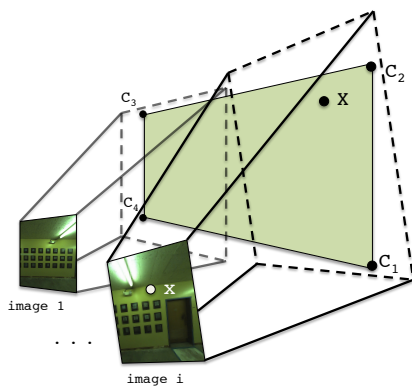


Figure 1: Planes are specified in 3D space by four corners C_1 to C_4 . Images are related to each plane through the camera matrices $P_{1..M}$.

at localization refinement, and demonstrates their inadequacies for our datasets. Section 4 presents our proposed approach to texture mapping, combining an improved localization refinement process with two image selection approaches. Section 5 contains results and conclusions.

2. Simple Texture Mapping

In all subsequent sections, we discuss the process of texture mapping a single plane, as the texturing of each of our planes is independent and can be completed in parallel.

The geometry of the texture mapping process for a plane is shown in Figure 1. As described earlier, we are provided with a set of M images with which we must texture our target plane. Each image has a camera matrix P_i for $i = 1..M$, which translates a 3D point in the world coordinate system to a 2D point or pixel in image i 's coordinates. If the 3D world point is not contained in the image, the 2D point will simply be outside of the image boundaries. A camera matrix P_i is composed of the camera's intrinsic parameters, such as focal length and image center, as well as extrinsic parameters which specify the rotation and translation of the camera's position in 3D world coordinates at the time that image i is taken. These extrinsic parameters are determined by the backpack hardware and localization algorithms mentioned earlier. A point X on the plane in 3D space can be related to its corresponding pixel x in image i through the following equation:

$$x = \text{project}(P_i X)$$

where

$$X = \begin{pmatrix} x \\ y \\ z \end{pmatrix} \text{ and } \text{project}(X) = \begin{pmatrix} x/z \\ y/z \end{pmatrix}$$

For the sake of simplicity, we treat all planes as rectangles by generating minimum bounding boxes for them. Since our final textures are stored as standard rectangular images anyway, we can simply leave the area between plane boundary and bounding box untextured, or crop it out as needed. A plane to be textured is thus defined by a bounding box with corners C_i in world coordinates and a normal vector indicating the front facing side of the plane. Our goal is to texture this plane using images captured by the backpack, while eliminating any visual discontinuities or seams that would suggest that the plane's texture is not composed of a single continuous image.

2.1. Direct Mapping

Ignoring the fact that the camera matrices $P_{1..M}$ are inaccurate, we can texture the plane by discretizing it into small square tiles, generally about 5 pixels across, and choosing an image to texture each tile with. We choose to work with rectangular units to ensure that borders between any two distinct images in our final texture are either horizontal or vertical. Since most environmental features inside buildings are horizontal or vertical, any seams in our texture intersect them minimally and are likely to be less noticeable.

In order to select an image for texturing tile t , we must first gather a list of candidate images that contain all four of its corners, which we can quickly check by projecting t into each image using the projection method above. Furthermore, each candidate image must have been taken at a time when its camera had a clear line-of-sight to t , which can be calculated using standard ray-polygon intersection tests between the camera location, the center of t , and other planes, all in world coordinates.

Once we have a list of candidate images for t , we must define a scoring function in order to compare images and objectively select the best one. Since camera localization errors compound over distance, we wish to minimize the distance between cameras used for texturing and our plane. Additionally, we desire images that are projected perpendicularly onto the plane, maximizing the resolution and amount of useful texture available in their projections.

These two criteria can be met by maximizing the function

$$\frac{1}{d} \cdot (-1 \cdot C) \cdot N$$

which minimizes camera angle α and distance d as shown in Figure 2.

As Figure 3 demonstrates, this approach leads to the best texture for each tile independently, but overall results in many image boundaries with abrupt discontinuities, due to significant misalignment between images.

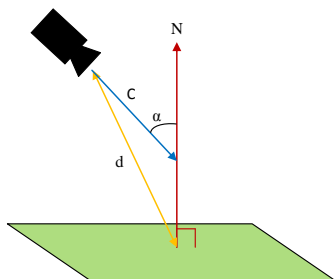


Figure 2: Images are selected by minimizing camera angle α and distance d .

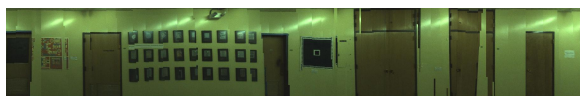


Figure 3: The result of direct texture mapping based on locally optimized textures.

2.2. Mapping with Caching

Since discontinuities occur where adjacent tiles select different images that do not align, it makes sense to take into account image selections made by neighboring tiles while selecting the best image for a given tile. By using the same image across tile boundaries, we eliminate the discontinuity altogether. If a tile is not visible in images chosen by its neighbors, using similar images is likely to result in less noticeable discontinuities.

Similar to a caching mechanism, we select the best image for a tile t by searching through two subsets of images for a good candidate, before searching through the entire set. The first subset of images is those selected by adjacent tiles that have already been textured. We must first check which images can map to t , and then of those, we make a choice according to the same scoring function in Figure 2. Rather than blindly reusing this image, we ensure it meets a threshold, which we set to $\alpha < 45^\circ$, to be considered a good image.

If no good image is found, we then check our second subset of images, which consists of images that were taken near the images in the first subset, both spatially and temporally. These images are not the same as the ones used for neighboring tiles, but they were taken at a similar location and time, suggesting that their localization and projection are very similar. Again, if no good image is found according to the same threshold, we then must search the entire set of candidate images.

The result of this caching approach is shown in figure 4. As compared to 3, discontinuities have been reduced overall, but the amount of remaining seams suggests that image selection alone cannot produce seamless textures. Camera

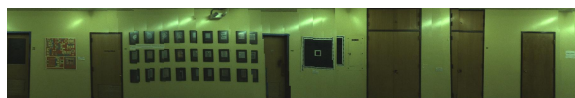


Figure 4: The result of adding a caching system to locally optimized textures.

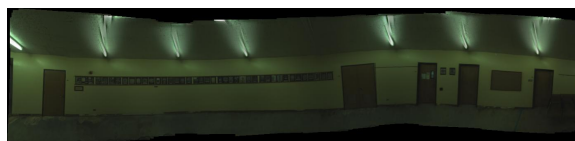


Figure 5: Image mosaicing.

matrices, or the image projections themselves have to be adjusted in order to reliably generate clean textures.

3. Existing Approaches to Image-Aligned Texture Mapping

In order to produce seamless texture mapping, either camera matrices need to be refined such that their localization is pixel accurate, resulting in a perfect mapping, or image stitching techniques need to be applied to provide this illusion. Before examining these approaches, we first obtain a set of images to work with.

Rather than perform camera or image adjustments across the many thousands of images acquired in a typical data collection, we opt to work with the more limited set of images corresponding to those chosen by the direct mapping approach, without caching. This set of images constitutes a good candidate set for generating a final seamless texture since it meets three important criteria. First, it contains at least one image that covers each tile on our plane; this ensures no holes in our final texture. Second, since images are all selected according to the same scoring function in Figure 2, they are taken at as much of a head-on angle as possible and should project onto the plane in similar ways. Third, as a side result of the scoring function, selected images are only good candidates for the tiles near their center of projection. Thus, there should be plenty of overlap between selected images, allowing for some degree of shifting without resulting in holes, as well as area for blending between them. With this set of images, we now review two existing approaches towards refining and combining their projections.

3.1. Image Mosaicing

When images of a plane are taken from arbitrary overlapping positions, they are related by homography [5]. Thus, existing homography-based image mosaicing algorithms are applicable [1]. However, errors can compound when long chains of images are mosaiced together using these



Figure 6: The graph-based localization refinement algorithm from [11] suffers from the problem of compounding errors.

approaches. For example, a pixel in the n th image in the chain must be translated into the first image’s coordinates by multiplying by the 3×3 matrix $H_1 H_2 H_3 \dots H_n$. Any error in one of these homography matrices is propagated to all further images until the chain is broken. For some chains of images this can happen almost immediately due to erroneous correspondence matches and the resulting image mosaic is grossly misshapen.

Figure 5 shows the output of the AutoStitch software package which does homography-based image mosaicing. This plane is nearly a best-case scenario with many features spread uniformly across it. Even so, the mosaicing produces errors that causes straight lines to appear as waves on the plane. This image was generated after careful hand tuning as well. Many planes that had fewer features simply failed outright. Thus, image mosaicing is not a robust enough solution for reliably texture mapping our dataset.

3.2. Image-Based 3D Localization Refinement

Another approach is to refine the camera matrices using image correspondences to guide the process. Each image’s camera matrix has 6 degrees of freedom that can be adjusted. Previous work on this problem attempted to refine camera matrices by solving a non-linear optimization problem [7]. This process is specific to the backpack system which generated our dataset, as it must be run during backpack localization [7, 2]. Unfortunately, this approach suffers from a similar error propagation problem shown in Figure 6.

4. Proposed Method for Seamless Texture Mapping

Our proposed approach towards texture mapping is a two-step process. First, with the same input set of images as described in Section 3, we perform image rotation and shifting in order to maximize SIFT feature matches between images. We then project these images onto our plane, applying textures either with the tile caching method from Section 2.2, or with the more specialized method described in Section 4.3.

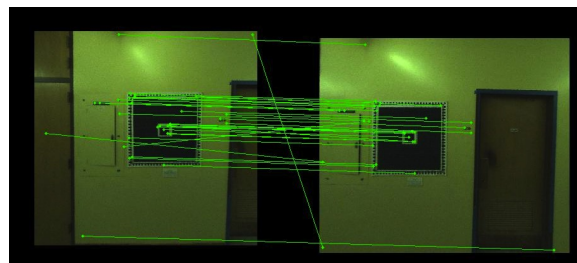


Figure 7: SIFT feature matches between overlapping images.

4.1. Image Projection and Rotation

Our localization approach begins with the projection of all our images onto separate copies of our plane, such that no projected data is covered up and lost. This is done in the same way as the approaches in Section 2. We then perform rotations on these projections, as adjacent images with different orientations will result in strong discontinuities.

These rotations are accomplished by using Hough transforms, which detect the presence and orientation of linear features in our images. Rather than match the orientation of such features in each image, we simply apply rotations such that the strongest near-vertical features are made completely vertical. This is effective for indoor models, since strong features in indoor scenes usually consist of parallel vertical lines corresponding to doors, wall panels, rectangular frames, etc. If features in the environment are not vertical, or are not parallel to each other, this step is skipped.

4.2. Robust SIFT Feature Matching using RANSAC

Our next step is to fix misalignment between overlapping images. We do this by first searching for corresponding points between all pairs of overlapping images using SIFT feature matching [8]. An illustration of this is given in Figure 7. The SIFT matches allow us to determine dx and dy distances between each pair of features for two images on the plane, determining where they should be projected relative to each other.

Since indoor environments often contain repetitive features such as floor tiles or doors, we need to ensure that our SIFT-based distances are reliable. In order to mitigate the effect of incorrect matches and outliers, the RANSAC framework [4] is used for a robust estimate of the optimal dx and dy distances between two images. The RANSAC framework handles the consensus-building machinery, and requires a fitting function and a distance function. For this application, the fitting function simply finds the average distance between matches in a pair of images. Our distance function for a pair of points is the difference between those points’ SIFT match distance and the average distance computed by the fitting function; we use a 10 pixel outlier

threshold. This means that a SIFT match is labeled as an outlier if its horizontal or vertical distance is not within 10 pixels of the average distance computed by the fitting function.

4.2.1 Refining Image Positions using Least Squares

There are a total of M^2 possible pairs of images, though we only generate distances between images that overlap at SIFT feature points. Given these distances and the original image location estimates, we can solve a least squares problem ($\min_{\vec{\beta}} \|X\vec{\beta} - \vec{\gamma}\|_2^2$) to estimate the correct location of the images on the plane. The M -dimensional vector $\vec{\beta}$ represents the unknown x and y locations of each image on the plane from $1 \dots M$. The optimal x and y locations are obtained in the same way, so we only consider the x locations here:

$$\vec{\beta} = (x_1, x_2, x_3, \dots, x_{M-1}, x_M)$$

The N by $(M+1)$ dimensional matrix X is constructed with one row for each pair of images with measured distances produced by the SIFT matching stage. A row in the matrix has a -1 and 1 in the columns corresponding to the two images in the pair. For example, the matrix below indicates that we generated a SIFT-based distance between images 1 and 2, images 1 and 3, images 2 and 3, etc.

$$X = \begin{pmatrix} -1 & 1 & 0 & \dots & 0 & 0 \\ -1 & 0 & 1 & \dots & 0 & 0 \\ 0 & -1 & 1 & \dots & 0 & 0 \\ \vdots & \vdots & \vdots & \ddots & \vdots & \vdots \\ 0 & 0 & 0 & \dots & 1 & 0 \\ 0 & 0 & 0 & \dots & -1 & 1 \\ 1 & 0 & 0 & \dots & 0 & 0 \end{pmatrix}$$

If only relative distances between images are included then there is no way to determine the absolute location of any of the images and the matrix becomes rank deficient. To fix this we choose the first image to serve as the anchor for the rest, meaning all the absolute distances are based on its original location. This is done by adding a row with a 1 in the first column and the rest zeros.

Finally, the N -dimensional observation vector $\vec{\gamma}$ is constructed using the SIFT-based distances generated earlier in the matching stage. The distances are denoted as $d_1 \dots d_N$ for N SIFT-based distances. The last element in the observation vector is the location of the first image determined by its original noisy localization, from [2, 7]:

$$\vec{\gamma}^T = (d_{1,2}, d_{1,3}, d_{2,3}, \dots, d_{N-2,N-1}, d_{N-1,N}, x_1)$$

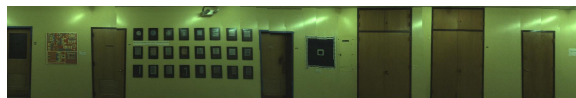


Figure 8: Localization refinement results in significantly fewer discontinuities in the final texture.

The $\vec{\beta}$ that minimizes $\|X\vec{\beta} - \vec{\gamma}\|_2^2$ results in a set of image locations on the plane that best honors all the SIFT-based distance measurements between images. In practice there are often cases where there is a break in the chain of images, meaning that no SIFT matches were found between one segment of the plane and another. In this case we add rows to the X matrix and observations to the $\vec{\gamma}$ vector that contain the original noisy x and y distance estimates generated by the localization algorithm [2, 7]. Another way to do this is to add rows for all neighboring pairs of images and solve a weighted least squares problem where the SIFT distances are given a higher weight i.e. 1, and the noisy distances generated by the localization algorithm [2, 7] are given a smaller weight i.e. 0.01.

After completing this same process for the y dimension as well, and making the resultant shifts, our images overlap and match each other with far greater accuracy. Applying the tile caching method from Section 2.2 on these re-localized images, results in the significant improvements shown in Figure 8.

4.3. Texture Mapping with Seam Minimization

As mentioned earlier, our backpack system has 2 cameras with 180° fisheye lenses facing to the right and left. Since the backpack operator only takes care to fully scan each wall and not necessarily the entirety of each ceiling and floor, cameras at higher angles with respect to plane normal vectors must be used for texturing large areas of floor and ceiling planes. These high camera angles translate into images that span extremely large areas once projected onto their planes. Such image projections have good scores (from Figure 2) for certain areas on the plane, but much worse scores for other areas. This can be seen in Figure ???. The tiling approach used in Section 2 was thus a good choice for texturing, as it allowed us to only use the parts of image projections that were good choices for their respective plane locations.

For wall planes however, we have images all taken from close distances and more head-on angles, and thus much smaller near-rectangular projections to work with. As a result, there is less deviation over the score of each tile within an image, as well as over the average scores of all images. This means that the scoring criteria from Figure 2 is less relevant to walls, which enjoy an abundance of head-on images.

Thus, for planes with optimal images, rather than select-

ing the set of best images, since all images are near in quality, we instead select the best set of images, such that the selection together results in the cleanest final texture. We will accomplish this by using entire images where possible, and defining a cost function to minimize the visibility of seams in our final texture.

4.4. Occlusion Masking

To begin with, we need to ensure that our images contain only content that should be mapped onto the target plane in question. The tiling approach used previously only checks occlusion for each tile as it is being textured. For our new approach, we use entire images, so we need to perform occlusion checks over the entirety of each image to determine available areas for texture mapping.

Fortunately, by virtue of our indoor environments, the vast majority of surface geometry is either horizontal or vertical, with high amounts of right angles. This means that after masking out occluded areas, our image projections will remain largely rectangular. We can thus be efficient by recursively splitting each image into rectangular pieces, and performing the same occlusion checks used in the tiling process where needed. To actually occlude out rectangles, we simply remove their texture, as we will ensure that untextured areas are never chosen for texture mapping.

4.5. Image Selection

To determine the set of images that results in the cleanest texture, we need a cost function to evaluate the visibility of seams between images in our set. A straightforward cost function that accomplishes this is the sum of squared pixel differences in overlapping regions between all pairs of images after they have been aligned as described in Section 4.1. Minimizing this cost function encourages image boundaries to occur either in featureless areas, such as bare walls, or in areas where images match extremely well.

With the cost function defined, we must now select the set of images for which the overall cost function is minimized. Since nearly all the images for our optimal case are head on, the best strategy to minimize seams is to choose as few images as possible while texturing a given plane. Thus, to cover the entirety of a plane, our problem can be defined as minimally covering a polygon i.e. the plane, using other polygons of arbitrary geometry i.e. our image projections, with the added constraint of minimizing our cost function between chosen images. This is a complex problem, though we can take a number of steps to simplify it. Given that our wall-texture candidate images are all taken from a head-on angle, and assuming only minor rotations are made during localization refinement, we can reason that their projections onto the plane are approximately rectangular, as in Figure ???. By discarding the minor excess texture and cropping them all to be rectangular, our problem

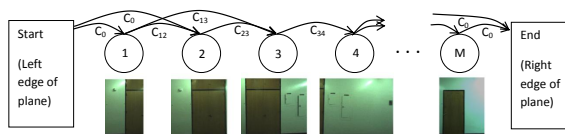


Figure 9: DAG construction for the image selection process.

becomes the conceptually simpler one of filling a polygon with rectangles, such that the sum of all edge costs between each pair of rectangles is minimal. We thus also retain the advantages of working with rectangular units, as explained in section 2.

The location and orientation of the cameras on our backpack is such that our images nearly always contain the entirety of the floor to ceiling range of wall planes. Images are therefore rarely projected with one above the other when texturing wall planes, which correspond to the optimal planes we are working with. In essence, we need only to ensure horizontal coverage of our planes, as our images provide full vertical coverage themselves. We can thus construct a Directed Acyclic Graph (DAG) from the images, with edge costs defined by our cost function above, and solve a simple shortest path problem to find an optimal subset of images with regard to the cost functions.

Figure 9 demonstrates the construction of a DAG from overlapping images of a long hallway. Images are sorted by horizontal location left to right, and become nodes in a graph. Directed edges are placed in the graph from left to right between images that overlap. The weights of these edges are determined by the cost functions discussed previously. Next, we add two artificial nodes, one start node representing the left border of the plane, and one end node representing the right border of the plane. The left(right) artificial node has directed edges with equal cost C_0 to (from) all images that meet the left(right) border of the plane.

We now solve the shortest path problem from the start node to the end node [3]. This provides a set of images completely covering the plane horizontally, while minimizing the cost of the seams between images.

In rare cases where the vertical dimension of the plane is not entirely covered by a chosen image, we are left with a hole where no image is chosen to texture.

SOMETHING HERE ABOUT CRAP CRAP

Rather than reverting to a 2D-coverage problem, we can elect to simply fill the hole by selecting images to fill it in a greedy fashion with respect to edge costs of the same cost function.

With this completed, we have now mapped every location on our plane to at least one image, and have minimized the number of images, as well as the discontinuity between their borders. In the next section, we apply blending between images where they overlap, but for the sake of com-



Figure 10: The tile caching approach is presented above the seam minimization approach.

parison with the unblended tile caching method in Section 2.2, we arbitrarily choose one image for texturing where images overlap. Figure 10 compares the tile caching method against this seam minimization method.

Though both methods provide quite accurate texturing thanks to the alignment process, the seam minimization approach results in fewer visible discontinuities, since it directly reduces the cost of each image boundary, while the tile caching method uses a scoring function that only approximates this effect. Furthermore, seam minimization guarantees the best selection of images, while the sequential tile caching method may select images early on that turn out to be poor choices once subsequent tiles have been processed.

In the context of the backpack modeling system, we apply the seam minimization approach on walls, due to its superior output when provided with head-on images. Floors and ceilings however, given their images taken at oblique angles, as shown in Figure ??, are textured using the tile caching method.

4.6. Blending

We now apply the same blending process on our two texturing methods: localization refinement followed by either tile caching or seam minimization.

Although our preprocessing steps and image selections in either method attempt to minimize all mismatches between images, there are unavoidable discontinuities due to different lighting conditions or inaccuracies in planar geometry or projection. These can however be treated and smoothed over by applying alpha blending over image seams. Whether the units we are blending are rectangularly-cropped images or rectangular tiles, we can apply the same blending procedure, as long as we have a guaranteed overlap between units to blend over.

For the tile caching method, we can ensure overlap by texturing a larger tile than needed for display. For example, for a rendered tile $l_1 \times l_1$, we can associate it with a texture $(l_1 + l_2) \times (l_1 + l_2)$ in size. For the seam minimization method, we have already ensured overlap between images. To enforce consistent blending however, it is beneficial to add a minimum required overlap distance while solving the shortest path problem in Section 4.5. If images overlap

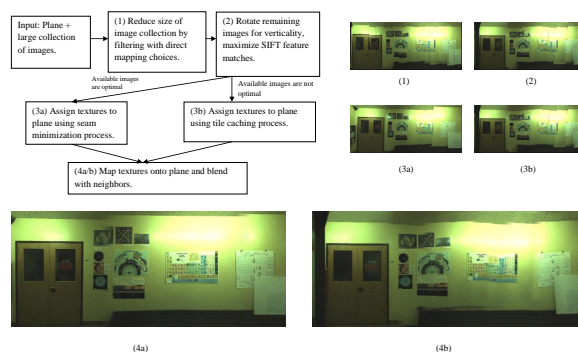


Figure 11: Our final texture processing pipeline, with the final output of both approaches.

in a region greater than the overlap distance, we only apply blending over an area equal to the overlap distance.

We apply alpha blending to blend pixels linearly across overlapping regions. Figure 11 shows our entire texture mapping pipeline and demonstrates the final blended output of both approaches.

5. Results and Conclusions

In this paper, we have developed an approach to texture map models with noisy camera localization data. We are able to refine image locations based on feature matching, and robustly handle outliers. We generalized one approach to texture mapping to any manner of planes and images, and successfully textured both simple rectangular walls as well as complex floor and ceiling geometry. We also presented an optimized texturing method that takes advantage of our localization refinement process and produces more seamless textures on planes where multiple head-on images are available. Each of these approaches is highly modular, and easily tunable for different environments and acquisition hardware.

Ceilings and floors textured with the tile caching approach, and walls textured with the seam minimization approach, are displayed in Figure 12. A more detailed walk-through demonstrating fully textured 3D models using the approaches in this paper is available in the accompanying video to this paper.

References

- [1] M. Brown and D. Lowe. Automatic panoramic image stitching using invariant features. *International Journal of Computer Vision*, 74(1):59–73, 2007. 3
- [2] G. Chen, J. Kua, S. Shum, N. Naikal, M. Carlberg, and A. Zakhor. Indoor localization algorithms for a human-operated backpack system. In *Int. Symp. on 3D Data, Processing, Visualization and Transmission (3DPVT)*. Citeseer, 2010. 1, 4, 5

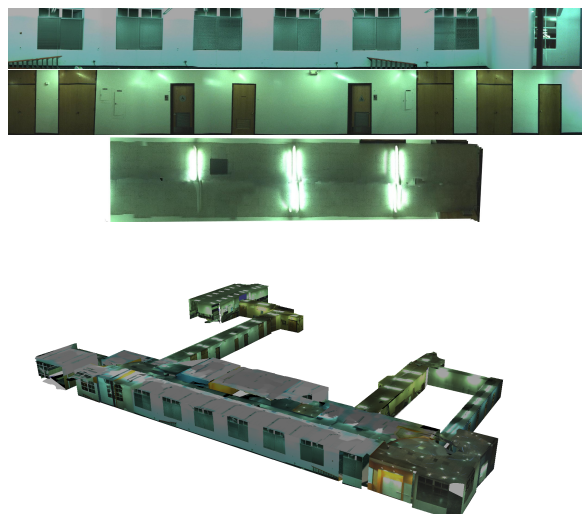


Figure 12: Examples of our final texture mapping output for walls, floors, and ceilings

- [3] E. Dijkstra. A note on two problems in connexion graphs. *Numerische Mathematik*, 1:269–271, 1959. 6
- [4] M. Fischler and R. Bolles. Random sample consensus: a paradigm for model fitting with applications to image analysis and automated cartography. *Communications of the ACM*, 24(6):381–395, 1981. 4
- [5] R. Hartley and A. Zisserman. *Multiple view geometry in computer vision*, volume 2. Cambridge Univ Press, 2000. 3
- [6] J. Kua, N. Corso, and A. Zakhor. Automatic loop closure detection using multiple cameras for 3d indoor localization. In *IS&T/SPIE Electronic Imaging*, 2012. 1
- [7] T. Liu, M. Carlberg, G. Chen, J. Chen, J. Kua, and A. Zakhor. Indoor localization and visualization using a human-operated backpack system. In *Indoor Positioning and Indoor Navigation (IPIN), 2010 International Conference on*, pages 1–10. IEEE, 2010. 1, 4, 5
- [8] D. Lowe. Object recognition from local scale-invariant features. In *Computer Vision, 1999. The Proceedings of the Seventh IEEE International Conference on*, volume 2, pages 1150–1157. Ieee, 1999. 4
- [9] V. Sanchez and A. Zakhor. Planar 3d modeling of building interiors from point cloud data. In *Internation Conference on Image Processing*, 2012. 1